

# Copolymerization with 2,4,6-Triaminopyrimidine for the Rolling-up the Layer Structure, Tunable Electronic Properties, and Photocatalysis of g-C<sub>3</sub>N<sub>4</sub>

Wingkei Ho,<sup>\*,†,⊥</sup> Zizhong Zhang,<sup>\*,†,‡</sup> Wei Lin,<sup>§</sup> Shuping Huang,<sup>||</sup> Xianwen Zhang,<sup>‡</sup> Xuxu Wang,<sup>‡</sup> and Yu Huang<sup>⊥</sup>

<sup>†</sup>Department of Science and Environmental Studies, The Hong Kong Institute of Education, Hong Kong, China

<sup>‡</sup>Research Institute Photocatalysis, State Key Laboratory of Photocatalysis on Energy and Environment, Fuzhou University, Fuzhou 350002, China

<sup>§</sup>Department of Chemistry & Biochemistry, University of California, San Diego, La Jolla, California 92093, United States

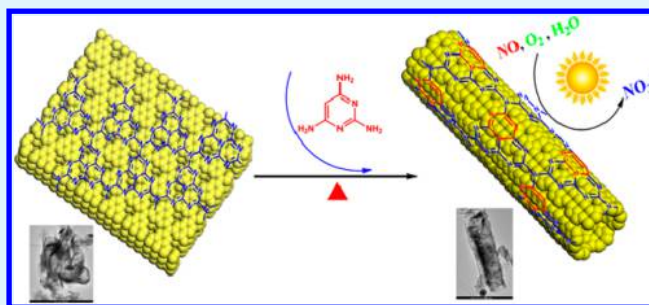
<sup>||</sup>Department of Chemistry, University of South Dakota, Vermillion, South Dakota 57069, United States

<sup>⊥</sup>Key Lab of Aerosol Chemistry & Physics and State Key Lab of Loess and Quaternary Geology, Institute of Earth Environment, Chinese Academy of Sciences, Xi'an 710075, China

## Supporting Information

**ABSTRACT:** Copolymerization with 2,4,6-triaminopyrimidine (TAP) is developed for precise substitution of one nitrogen with carbon atom in the triazine ring of polymeric g-C<sub>3</sub>N<sub>4</sub>. Direct incorporation of C<sub>4</sub>N<sub>2</sub> ring from TAP into the network retains the structural features of g-C<sub>3</sub>N<sub>4</sub>, but induces the rolling-up of g-C<sub>3</sub>N<sub>4</sub> sheets into tubular configuration. The band gap energy is narrowed from 2.7 to 2.4 eV by a negative shift of valence band of the g-C<sub>3</sub>N<sub>4</sub> photocatalyst, which enhances charge-carrier migration and separation, leading to higher photocatalytic activity for NO gas pollutant removal. It is attributed to the decrease of the  $\pi$ -deficiency and the generation of imbalanced electron density in  $\pi$ -electron conjugated units of g-C<sub>3</sub>N<sub>4</sub> by TAP incorporation. This work provides a significant technique for precise control of heteroatom in the framework of g-C<sub>3</sub>N<sub>4</sub> to finely adjust its intrinsic electronic properties and its photocatalytic properties.

**KEYWORDS:** g-C<sub>3</sub>N<sub>4</sub>, copolymerization, nitrogen substitution, tubular configuration, photocatalysis



## 1. INTRODUCTION

Artificially mimicking photosynthesis for efficient solar energy conversion motivates the searches for powerful multifunctional materials as photocatalysts working under visible light. Graphitic carbon nitride (g-C<sub>3</sub>N<sub>4</sub>) has been receiving much attention as a noble metal-free and visible-light-driven photocatalyst that has versatile properties and promising applications, such as H<sub>2</sub> evolution from water, degradation of organic dyes, selective organic transformations to fine chemicals, and CO<sub>2</sub> conversions.<sup>1–6</sup> Nevertheless, the pristine g-C<sub>3</sub>N<sub>4</sub> photocatalyst suffers more severely from fast charge recombination and lack of absorption above 460 nm,<sup>7</sup> which inevitably restrict its widespread applications. The resolution of these scientific issues is dependent on the fine-tuning of intrinsic electronic structures to narrow the band gap and reduce electron–hole recombination rates to improve the photocatalytic performance of g-C<sub>3</sub>N<sub>4</sub>.

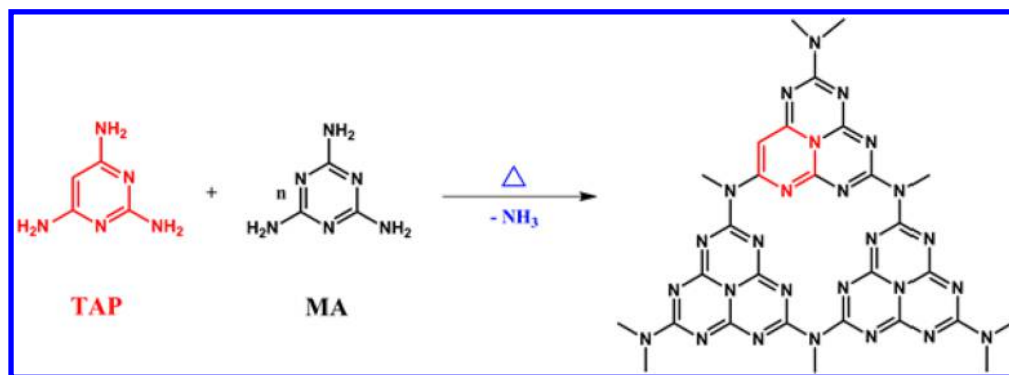
Various approaches have been developed to manipulate the electronic structure of g-C<sub>3</sub>N<sub>4</sub>. These approaches include thermal condensation, heteroatom doping, copolymerization,

and semiconductor hybridization,<sup>8–14</sup> among which heteroatom doping is regarded as the most popular method for this purpose because of the organic nature of g-C<sub>3</sub>N<sub>4</sub>, which allows for plentiful organic schemes to engineer molecular structure. Nonmetal elements, such as sulfur, carbon, phosphorus, boron, fluorine, and iodine,<sup>15–20</sup> have been introduced into g-C<sub>3</sub>N<sub>4</sub> framework to successfully extend visible light absorption and accelerate photogenerated electron–hole separation. However, the effect of heteroatom doping on the photocatalytic performance of g-C<sub>3</sub>N<sub>4</sub> is frequently affected by the prepared methods and the selected ligands. For example, boron-modified g-C<sub>3</sub>N<sub>4</sub> prepared from the 1-butyl-3-methylimidazolium tetrafluoroborate (BmimBF<sub>4</sub>) is virtually inactive for water splitting,<sup>21</sup> whereas boron-modified g-C<sub>3</sub>N<sub>4</sub> prepared from sodium tetraphenylboron (Ph<sub>4</sub>BNa) shows much higher activity for H<sub>2</sub> production than pure g-C<sub>3</sub>N<sub>4</sub> catalyst.<sup>22</sup> This

Received: January 5, 2015

Accepted: February 23, 2015

Published: February 23, 2015

Scheme 1. Incorporation of TAP into the Network of g-C<sub>3</sub>N<sub>4</sub>

is because controlling heteroatoms in the particular site of the network of g-C<sub>3</sub>N<sub>4</sub> is difficult. Therefore, precise control of heteroatom in the framework of g-C<sub>3</sub>N<sub>4</sub> remains to be a challenge, but it is very important for the fine-tuning of its intrinsic electronic structures, and thus its photocatalytic properties.

The perfect g-C<sub>3</sub>N<sub>4</sub> is constructed from the repeating units of N-bridged “poly(tri-s-triazine)” to form  $\pi$ -conjugated graphitic plane. Although g-C<sub>3</sub>N<sub>4</sub> has a similar layered structure with graphite, the electrical conductivity of g-C<sub>3</sub>N<sub>4</sub> is significantly lower than that of graphene.<sup>23</sup> This is attributed to a symmetrical substitution of high-electronegativity nitrogen atoms for carbon atoms in the carbon ring that leads to an increase in the  $\pi$ -deficiency of the conjugated system, and thus decrease the electron availability of g-C<sub>3</sub>N<sub>4</sub> compared with graphene. From this point of view, to enhance electrical conductivity and subsequently suppress the recombination of photogenerated charge carriers for g-C<sub>3</sub>N<sub>4</sub>, an ideal strategy is to partially reversely substitute the nitrogen atom with low-electronegativity atoms, such as carbon, to decrease  $\pi$ -deficiency and extend the  $\pi$ -electron conjugated system to narrow the band gap energy of g-C<sub>3</sub>N<sub>4</sub> for harvesting visible light. Although Dong et al. had synthesized carbon doped g-C<sub>3</sub>N<sub>4</sub> by copolymerization of the melamine pretreated with absolute ethanol as the precursor, and suggests that the replacement of bridging N among triazine units with doping C,<sup>16</sup> it is hard to control the content and the site of the carbon to dope into the skeleton structure of triazine of g-C<sub>3</sub>N<sub>4</sub>.

In this study, 2,4,6-triaminopyrimidine replacement of melamine was successfully copolymerized into the network of g-C<sub>3</sub>N<sub>4</sub> for precise substitution of nitrogen in the skeleton of tri-s-triazine with carbon (Scheme 1). The introduction of C<sub>4</sub>N<sub>2</sub> ring from TAP molecular into the C<sub>3</sub>N<sub>4</sub> structure facilitated the decrease of the  $\pi$ -deficiency and the generation of imbalanced electron density in  $\pi$ -electron conjugated units of g-C<sub>3</sub>N<sub>4</sub>. The rolling-up of g-C<sub>3</sub>N<sub>4</sub> sheet into the tubular configuration after TAP incorporation was first observed. Moreover, the resultant g-C<sub>3</sub>N<sub>4</sub> displayed the tunable band gap and efficient separation of photogenerated charge carriers, which results in efficient photocatalytic activity for NO gas pollutants removal. This design is a significant step toward the fine-tuning of intrinsic electronic structures and photocatalytic properties of polymeric g-C<sub>3</sub>N<sub>4</sub>. It provides a flexible choice for controlling heteroatom doping in the specific site of the network of g-C<sub>3</sub>N<sub>4</sub>.

## 2. EXPERIMENTAL SECTION

**2.1. Sample Preparation.** The modified g-C<sub>3</sub>N<sub>4</sub> samples were prepared through copolymerization of melamine (MA) and 2,4,6-triaminopyrimidine (TAP). In a typical preparation steps, 10 g MA and a certain amount of TAP were mixed uniformly in an agate mortar. Then, the mixture was placed in a porcelain crucible with a cover and heated at 5 °C min<sup>-1</sup> up to 550 °C for 4 h. The resulting samples were labeled as *x* TAP-CN (*x* denotes the TAP/MA molar ratio, *x* = 0.5, 1, 2, 3, and 10%, respectively).

**2.2. Characterization.** C, N, and H contents were measured using an Elementar Vario EL analyzer. X-ray diffraction (XRD) measurements were performed on a Bruker D8 Advance X-ray diffractometer using Cu K $\alpha$  radiation ( $\lambda$  = 1.5406 Å). BET measurements were carried out using Micrometrics ASAP 2020 surface area/porosity analyzer. UV-vis spectra were recorded through a Varian Cary 500 Scan UV-vis-NIR spectrophotometer using a BaSO<sub>4</sub> standard. FTIR spectra were obtained using a Nicolet Magna 670 FTIR spectrometer that has a DTGS detector. EPR spectra were recorded using a Bruker A-300-EPR X-band spectrometer at room temperature. XPS spectra were obtained using a VG ESCALAB 250 XPS system that has a monochromatized Al K $\alpha$  X-ray source (15kV, 200 W, 500  $\mu$ m pass energy = 20 eV). All binding energies were referenced to the C 1s peak at 284.6 eV of the surface adventitious carbon. Photocurrent measurements were conducted in a BAS Epsilon Electrochemical System with a conventional three-electrode cell using a Na<sub>2</sub>SO<sub>4</sub> (0.2 mol L<sup>-1</sup>) electrolyte solution.

**2.3. Photocatalytic Measurements.** The photocatalytic activity was measured by removing NO at 600 ppb levels using a continuous flow reactor at ambient temperature. The volume of the rectangular reactor, which was made of stainless steel and covered with quartz glass window, was 4.5 L (30 cm  $\times$  15 cm  $\times$  10 cm). A 30 W visible LED was vertically placed outside the reactor and was used as a light source. Photocatalyst (0.1 g) was coated onto a dish with a diameter of 12.0 cm. The coated dish was then pretreated at 70 °C to remove water in the suspension. The NO gas was acquired using a compressed gas cylinder at an NO (N<sub>2</sub> balance) concentration of 50 ppm. It was diluted to about 600 ppb through a dynamic gas calibrator (Ecotech GasCal 1000) that was combined with a zero air supply. The gas flow rate through reactor was controlled at 1000 mL/min using a mass flow controller. The lamp was turned on after obtaining the adsorption-desorption equilibrium. The concentration of NO was continuously measured using a NOx analyzer model T200 (Teledyne API). The removal ratio ( $\delta$ ) of NO was calculated as  $\delta(\%) = (1 - C/C_0) \times 100\%$ , where *C*<sub>0</sub> is the initial concentration of NO and *C* is the concentration of NO after the photocatalytic reaction.

## 3. RESULTS

**3.1. Synthesis and Structural Characterization.** The incorporation of TAP into the framework of g-C<sub>3</sub>N<sub>4</sub> conjugated system is depicted in Scheme 1. The TAP has a molecular structure similar to MA; both of them possess a six-membered aromatic heterocycle with 2,4,6-triamine. The only difference in

the molecular structure was that MA has a 1,3,5-triazine skeleton ( $C_3N_3$ ), whereas the TAP molecular consists of pyrimidine with two nitrogen atoms in the ring ( $C_4N_2$ ). TAP can easily substitute precursor MA and implant into the network of  $g-C_3N_4$  because of the high similarity between the molecular structures of AM and TAP. Therefore, the molar ratio of C to N was gradually increased with more TAP incorporation through bulk element analysis, as shown in Table 1. For example, the C/N molar ratio was increased from 0.676

**Table 1. Bulk C, N, and H Contents, BET Specific Surface Area, and Band Gap Energy ( $E_g$ ) of the  $g-C_3N_4$  Samples**

samples	N (%)	C (%)	H (%)	C/N	H/C	BET ( $m^2/g$ )	$E_g$ (eV)
$g-C_3N_4$	60.68	35.05	1.567	0.674	0.536	39.1	2.69
0.5% TAP	60.08	34.87	1.658	0.677	0.571	37.5	2.63
1%TAP	59.46	34.57	1.731	0.678	0.601	37.2	2.59
2%TAP	59.20	34.59	1.782	0.682	0.618	29.4	2.54
3%TAP	58.65	34.55	1.842	0.687	0.640	26.5	2.50
10% TAP	56.98	34.89	1.963	0.714	0.675	25.8	2.39

for pristine  $g-C_3N_4$  to 0.714 for 10% TAP-CN. Moreover, the H/C molar ratio was correspondingly increased by incorporating TAP. The increased extent of C/N molar ratio for the 10% TAP-CN samples was calculated to be about 5.93% compared with the pristine  $g-C_3N_4$ . This result is consistent with the theoretical value of 5.98% for 10% TAP incorporation, which indicates successful incorporation of TAP into the network of  $g-C_3N_4$ . The additional characterizations below by IR and XPS also confirmed the successful incorporation.

The characteristic structure of heptazine units was analyzed through FTIR spectra to investigate the effect of TAP incorporation on the heptazine units of  $g-C_3N_4$ , as shown in Figure 1. The multiple bands of the pristine  $g-C_3N_4$  between

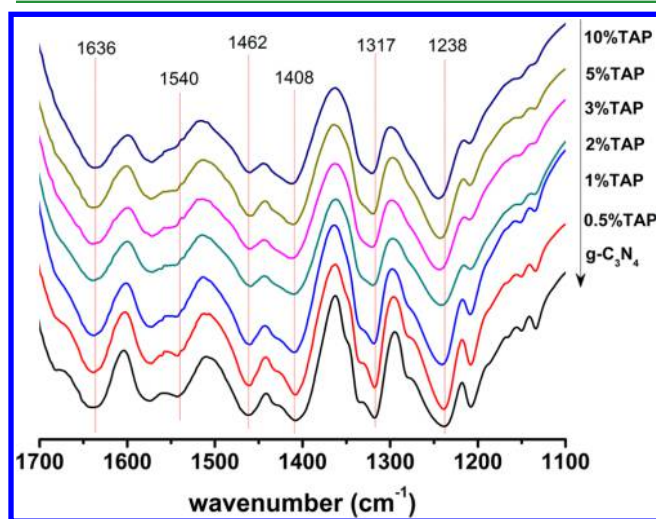


**Figure 1.** FTIR spectra of the pristine and modified  $g-C_3N_4$  samples.

1200–1600  $cm^{-1}$  corresponded to the characteristic absorbance of the typical aromatic CN heterocycles. The absorption peaks at 1636 and 1540  $cm^{-1}$  were due to  $C=N$  bonds, whereas the peaks at 1317 and 1238  $cm^{-1}$  were attributed to single  $C-N$  bonds.<sup>24</sup> When copolymerized with TAP, the characteristic absorbance for the graphitic CN heterocycles

remained almost unchanged. This suggested that the TAP incorporation did not severely alter either the bulk structure or the core chemical skeleton of  $g-C_3N_4$ . However, the intensity was weakened by the increase of TAP. Moreover, the IR peak at 1238  $cm^{-1}$  shifted to higher frequencies when TAP content increased. The shifts indicated that the enhanced strength of  $C-N$  covalent bonds resulted in higher frequencies. These findings were due to the electronegativity of the carbon that was lower than that of nitrogen, which resulted in the enhancement of the adjacent  $C-N$  covalent bonds in heptazine units. Thus, TAP monomers were successfully substituted for melamine and copolymerized into the framework of heptazine units.

Figure 2 shows the XPS spectra to determine the effect of TAP incorporation on the chemical skeleton of  $g-C_3N_4$ . The modified  $g-C_3N_4$  displays that the C 1s and N 1s XPS peak shapes were almost similar to that of the parent  $g-C_3N_4$  samples. However, the binding energy for the C 1s XPS at 287.9 eV ascribed to  $C-(N)_3$  bonding shifted slightly to lower energy, and the peak at 286.1 eV corresponded to  $C-N$  reversely shift to higher energy when TAP incorporation increased.<sup>25</sup> The C/N molar ratios were calculated from XPS spectra, as shown in Table 2. The C/N ratios gradually increased as TAP increased, which is consistent with the result of the incorporation of TAP into  $g-C_3N_4$ .

The main N 1s XPS of the parent  $g-C_3N_4$  can be fitted into three peaks at 398.5, 399.8, and 400.9 eV. These three peaks corresponded to N bonded to carbon atoms ( $C=N-C$ ) of triazine rings (denoted as N1), the tertiary N in the form of  $N-(C)_3$  (denoted as N2, as shown in Figure 2 inset), and amino functional groups ( $C-N-H$ ),<sup>26,27</sup> respectively. Upon incorporation with TAP, the binding energy for the N 1s XPS peaks did not obviously change. However, the N1/N2 molar ratios decreased when TAP content increased (Table 2), which is consistent with the result of the substitution of partial N1 atoms by carbon atom in the framework of  $g-C_3N_4$  when MA was substituted by TAP. Therefore, TAP monomers were successfully substituted for melamine and incorporated into the framework of heptazine units.

The crystal structure of the TAP-incorporated  $g-C_3N_4$  was investigated through XRD pattern, as shown in Figure 3. All samples revealed typical graphitic layered structures without an impurity phase. However, the X-ray diffraction peak was obviously decreased and broadened upon TAP incorporation, compared with that of the pristine  $g-C_3N_4$ . Therefore, the graphitic structure was disturbed by TAP incorporation. Furthermore, the main peak at 27.75° for the pristine  $g-C_3N_4$  displayed a slight shift to lower angles with TAP incorporation (Figure 3B), indicating an increase in the interplanar distance of graphitic layered structure. The 2-theta angle continuously decreased from 27.75 to 27.53° because of the gradual increase of TAP content from 0.5 to 3%, which corresponded to the increase of the interplanar distance from 0.321 nm for the pristine  $g-C_3N_4$  to 0.324 nm among the 3% TAP-CN samples. The increase in the interplanar distance facilitated the reactant molecule's approach to the interplanar space to improve the photocatalytic reaction. However, the  $2\theta$  angle increased when the TAP content was further increased to 5 and 10%. Therefore, the incorporation of 3% TAP in  $g-C_3N_4$  caused the maximum interplanar distance of the graphitic layered structure. Evidently, TAP incorporation has a significant influence on the planar structure of  $g-C_3N_4$ , and may improve the semiconductive properties of  $g-C_3N_4$ . The  $N_2$  absorption–

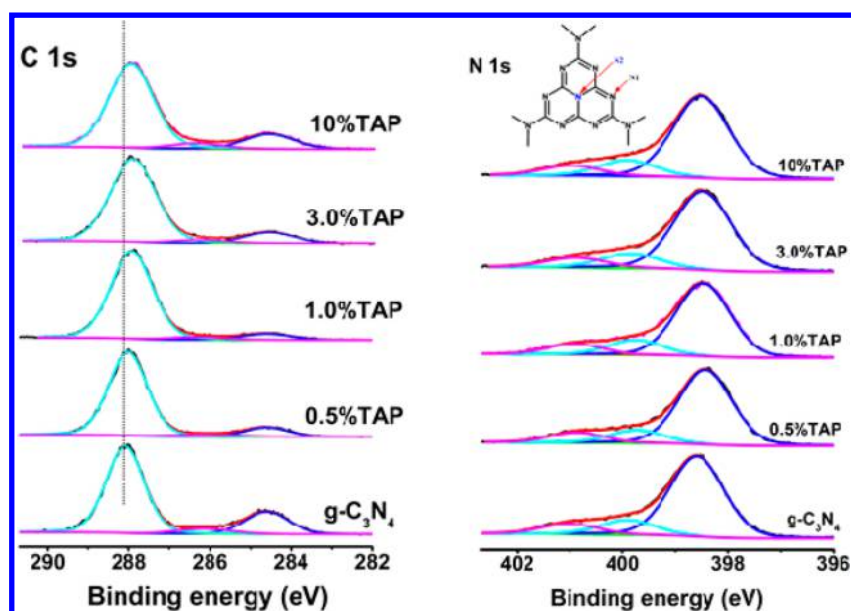


Figure 2. XPS of the pristine and modified  $g\text{-C}_3\text{N}_4$  samples.

Table 2. Estimated C/N Ratios and Different N Species Ratios for the Modified  $g\text{-C}_3\text{N}_4$  Samples

samples	$g\text{-C}_3\text{N}_4$	0.5%TAP	1%TAP	3%TAP	10%TAP
C/N	0.749	0.752	0.765	0.788	0.811
N1/N2 <sup>a</sup>	5.58	5.51	5.34	5.23	5.04

<sup>a</sup>N1 and N2 corresponding to N species at 398.5 and 399.8 eV of N 1s XPS spectra, respectively.

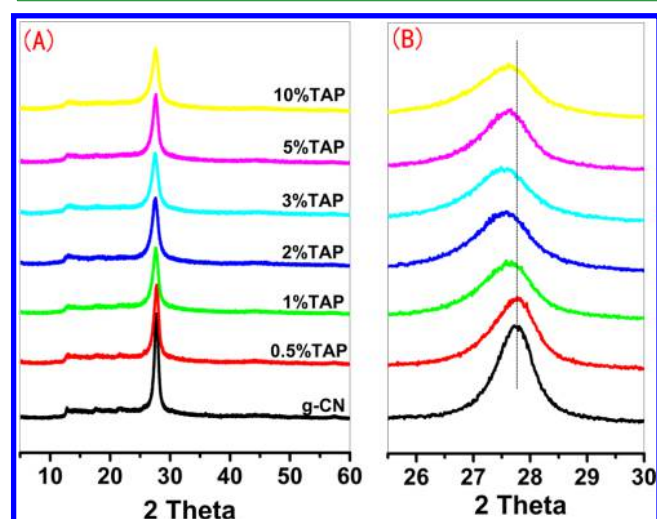


Figure 3. (A) XRD patterns of the TAP-incorporated  $g\text{-C}_3\text{N}_4$  samples; (B) enlarged view of main peak at around  $27.75^\circ$ .

desorption isotherms of the samples were measured and the specific surface area was calculated, as shown in Table 1. The BET surface area was gradually decreased when the TAP incorporation was increased because of the improvement of degree of thermal condensation of  $g\text{-C}_3\text{N}_4$  after TAP incorporation.

The microstructure of the as-prepared samples was investigated by TEM, as shown in Figure 4 and Figure S1 in the Supporting Information. A typical thick and sheetlike structure was clearly observed in the pristine  $g\text{-C}_3\text{N}_4$  (Figure

4a). Interestingly, the  $g\text{-C}_3\text{N}_4$  layer self-organized into nanotubes with a wrinkled appearance when the TAP was incorporated. The configuration of tubular structure is depended on the TAP contents. For 0.5% TAP, the layer was partially rolled up into the half-round nanotube (Figure 4b). When the TAP content was increased to 1%, the layers was assembled into the intact nanotube with diameters of approximately  $1\ \mu\text{m}$  (Figure 4c). Further increasing incorporation to 2% or more TAP, the nanotube configuration was begun to be collapsed (Figure 4d and Figure S1 in the Supporting Information). The SEM images (Figure S2 in the Supporting Information) of 1% TAP-CN also confirm the tube morphology of  $g\text{-C}_3\text{N}_4$  after TAP incorporation. It is worth to note that TAP incorporation induces the rolling-up of  $g\text{-C}_3\text{N}_4$  sheets to form nanotubes. Since the aromaticity of pyrimidine ring of TAP molecular was comparatively higher than that for s-triazine of MA, the TAP substitution of precursor MA integrated into the network of  $g\text{-C}_3\text{N}_4$  resulting in higher electronic density of the modified  $\text{C}_6\text{N}_8$  units in comparison with that of the pristine  $g\text{-C}_3\text{N}_4$ . The imbalance of electron density in the modified  $\text{C}_6\text{N}_8$  units may contribute to the rolling-up of  $g\text{-C}_3\text{N}_4$  sheets and subsequent formation of the nanotube configuration.

**3.2. Optical and Electronic Properties.** Figure 5 shows the UV-vis absorption spectra of  $g\text{-C}_3\text{N}_4$  functionalized with various contents of TAP. The parent  $g\text{-C}_3\text{N}_4$  showed a band edge absorption at ca. 461 nm with a broad absorption shoulder extending into 600 nm, which was consistent with the results reported in the previous literature on  $g\text{-C}_3\text{N}_4$  samples that were prepared through thermal condensation in air.<sup>28</sup> A red shift of the band edge absorption and an increase of more than 460 nm in the absorption shoulder occurred along with TAP incorporation. The extent of the red shift of the band edge absorption was gradually increased when the amount of TAP incorporation was increased. Thus, the electronic structure of  $g\text{-C}_3\text{N}_4$  was remarkably modified by the incorporation of TAP. The band gap energy ( $E_g$ ) of  $g\text{-C}_3\text{N}_4$  samples was calculated through the equation  $E_g = hc/\lambda$ , where  $\lambda$  is the wavelength (nm) obtained from the tangent drawn from the absorbance curve. The calculated band gap energy is shown in Table 1.  $E_g$

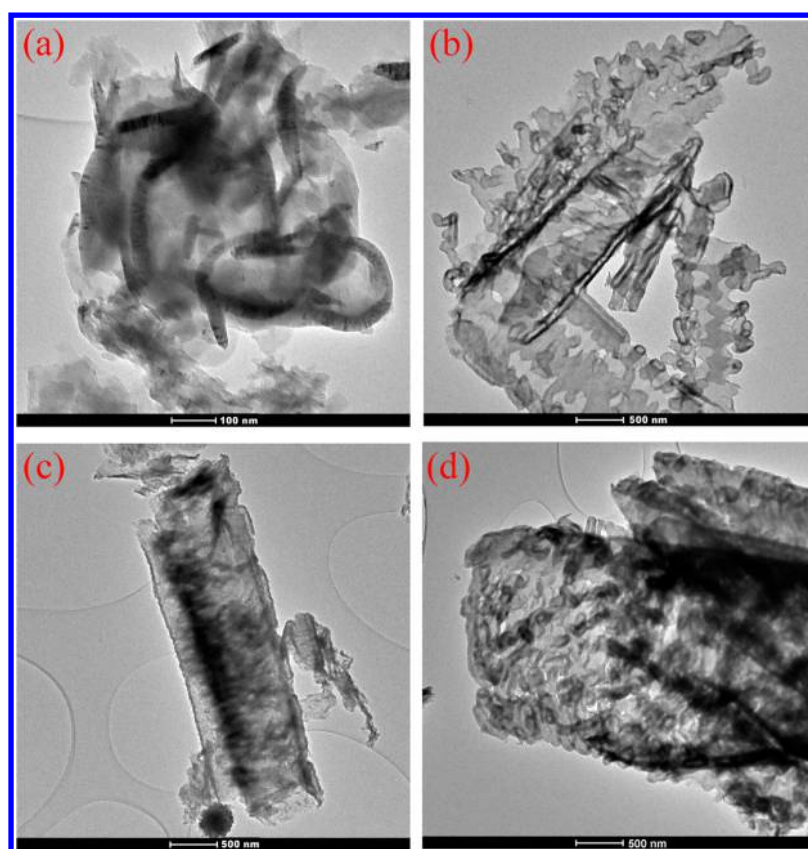


Figure 4. TEM images for (a)  $g\text{-C}_3\text{N}_4$ , (b) 0.5%TAP-CN, (c) 1%TAP-CN, and (d) 2%TAP-CN.

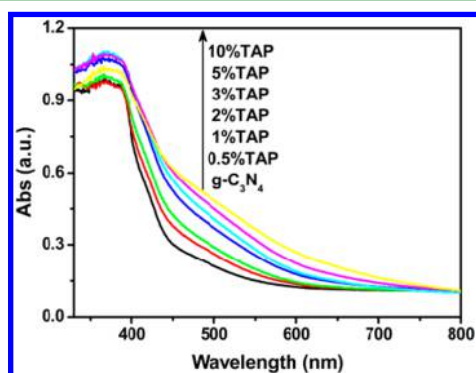


Figure 5. UV-visible light absorption spectra of the pristine and modified  $g\text{-C}_3\text{N}_4$  samples.

was remarkably decreased from 2.69 eV for the pristine  $g\text{-C}_3\text{N}_4$  to 2.59 eV for the 1% TAP to 2.39 eV for the 10% TAP incorporation. The  $E_g$  narrowing arose from the introduction of TAP into the network to decrease the  $\pi$ -deficiency and efficiently extend the conjugated  $\pi$ -electron system.

The total and partial density of states (DOS) of the pristine and modified  $g\text{-C}_3\text{N}_4$  were carried out via Heyd-Scuseria-Ernzerhof (HSE06) functional with Hartree-Fock exchange mixing parameter  $a = 0.175$  (Figure 6 and Supporting Information).<sup>29</sup> The calculated band gap for the pristine  $g\text{-C}_3\text{N}_4$  was 2.7 eV, where HOMO was predominantly derived from nitrogen 2p orbital (mainly  $2P_z$ ), whereas LUMO consisted mainly of carbon 2p orbitals ( $2P_y$ ), which was consistent with the corresponding literature data.<sup>1</sup> The incorporation of TAP for the precise substitution of nitrogen with carbon atom in the triazine ring resulted in the narrowing

of band gap by a negative shift of HOMO level, whereas LUMO still retained. For example, 6% TAP incorporation in the model evidently caused the negative shift of HOMO with 0.2 eV, decreasing the band gap to 2.5 eV (Figure 6b), which matched well with the observed values from the UV-vis absorption spectra. Doping of carbon from TAP broke the balance of the electron density on the corresponding triazine rings. Subsequently, the HOMO of 6% TAP-CN monolayer was dominated with  $2P_y$  orbitals of the substituted carbon and the nitrogen ( $N_2$ )  $2P$  orbitals to decrease  $\pi$ -deficiency of  $g\text{-C}_3\text{N}_4$  system (see Figure 6b). The imbalanced  $\pi$ -conjugated electrons then induced the negatively shift of the HOMO. With the increasing proportion of TAP, the contributions of substituted carbon would decrease the balances of the  $\pi$ -conjugated electrons on the triazine rings, and accordingly reduced the band gaps on the large doping compounds as observed in the UV-vis absorption spectra. Since the TAP incorporation kept the position of the LUMO level unchanged, the potential of the conduction band electron of  $g\text{-C}_3\text{N}_4$  was sufficient to reduce oxygen to produce active oxygen species for the oxidation reaction. Hence, these calculations indicated that TAP incorporation narrow the band gap energy of  $g\text{-C}_3\text{N}_4$  for more visible-light harvesting and might enhance photocatalytic oxidation of NO.

**3.3. Photocatalytic Activity.** Gas-phase photocatalytic oxidation of NO through a continuous flow model was used to evaluate the effect of TAP incorporation on the photocatalytic behavior of catalyst samples under visible light LED irradiation. The dependence of the concentration of NO as a function of reaction time is shown in Figure 7A. The amount of NO rapidly decreased from 605 to 362 ppb over the pristine  $g\text{-C}_3\text{N}_4$  samples under visible light LED irradiation. NO concentration

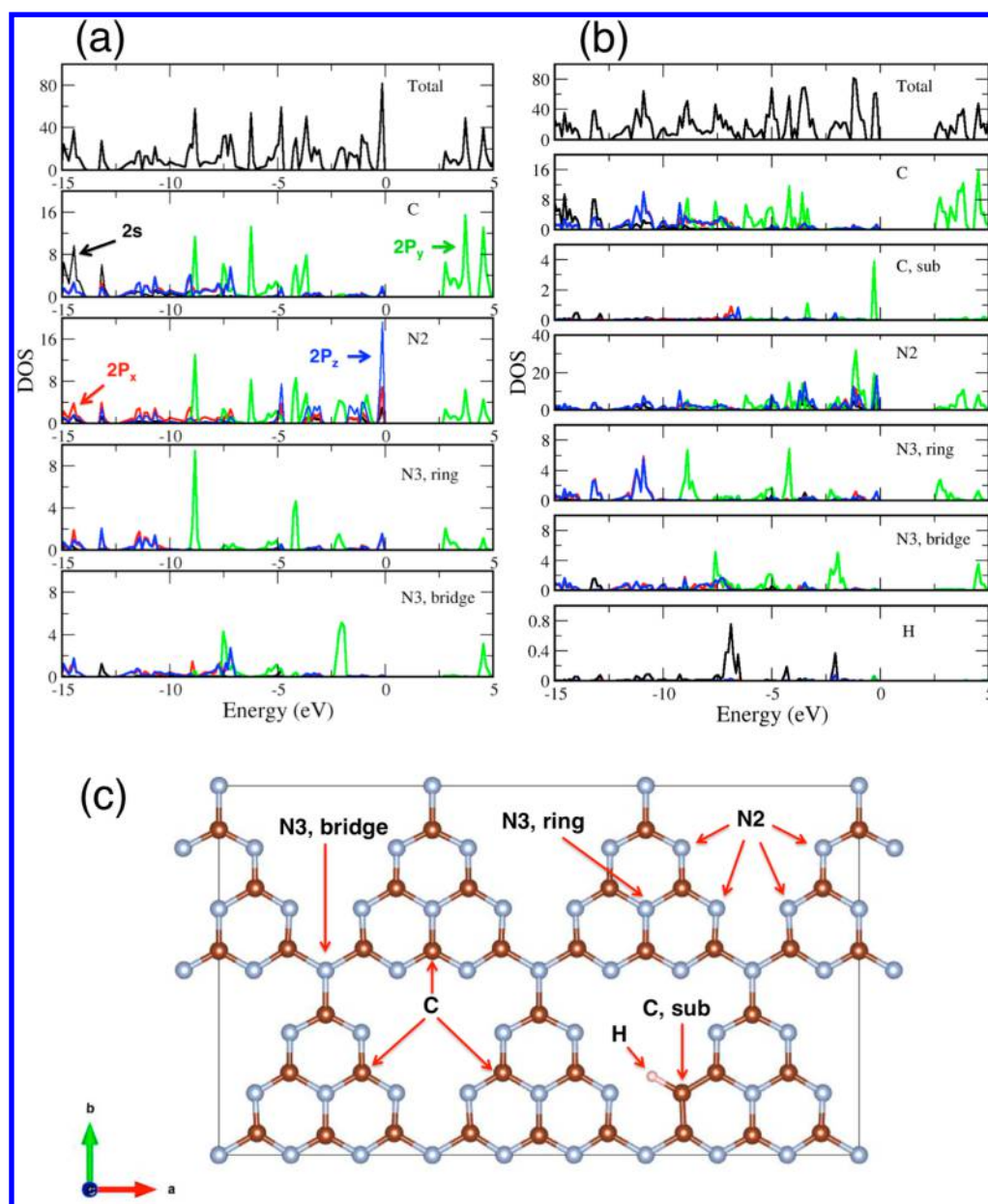


**Figure 6.** Calculated total and partial density of states (DOS) of the (a) pristine  $g\text{-C}_3\text{N}_4$  and (b) 6% TAP-CN; (c) unit cell of 6% TAP-CN  $g\text{-C}_3\text{N}_4$  monolayer in calculations.

was further diminished to 245 ppb when 1% of TAP was incorporated in the reaction system.  $\text{NO}_3^-$  ion products of NO oxidation accumulated on the 1% TAP-CN catalyst surface were observed by XPS (Figure S3 in the Supporting Information). NO degradation over the TAP polymer as a controlled experiment was also carried out. No activity was observed on the TAP polymer. Therefore, TAP incorporation can efficiently improve the photocatalytic properties of  $g\text{-C}_3\text{N}_4$ . The dependence of NO removal on the content of TAP incorporation was investigated in detail and shown in Figure 7B. NO removal significantly increased from 40 to 59.4% when TAP was increased from 0 to 1%. NO removal nearly reached a constant when the content of TAP was increased from 1 to 3%. However, NO removal exhibited an abrupt decline when the content of TAP was increased to 5 or 10%. The most optimum TAP contents seem to be in the range of 1 to 3%. The stability of the functionalized catalysts for NO removal was also

investigated. Figure 8 shows the prolonged-run experiments for NO removal over the optimized 1% TAP-CN catalyst. Interestingly, 1% TAP-CN can maintain efficient and durable visible light photocatalytic activities after six cycles of repeated runs with no obvious deactivation. The stability of the 1% TAP-CN catalyst was further confirmed by FT-IR spectra after the prolonged runs (Figure S4 in the Supporting Information). Thus, the TAP-CN photocatalyst is both stable and efficient, which is important for practical applications.

The photocatalytic activity of the modified  $g\text{-C}_3\text{N}_4$  was significantly improved compared with that of the pristine  $g\text{-C}_3\text{N}_4$ . However, the TAP incorporation retained the structural features and induced decrease in the BET surface area of  $g\text{-C}_3\text{N}_4$ . The results closely depended on the fundamental properties of charge-carrier migration and separation in the TAP-incorporated  $g\text{-C}_3\text{N}_4$ . Photoluminescence spectra (PL) were employed to determine the separation/recombination of

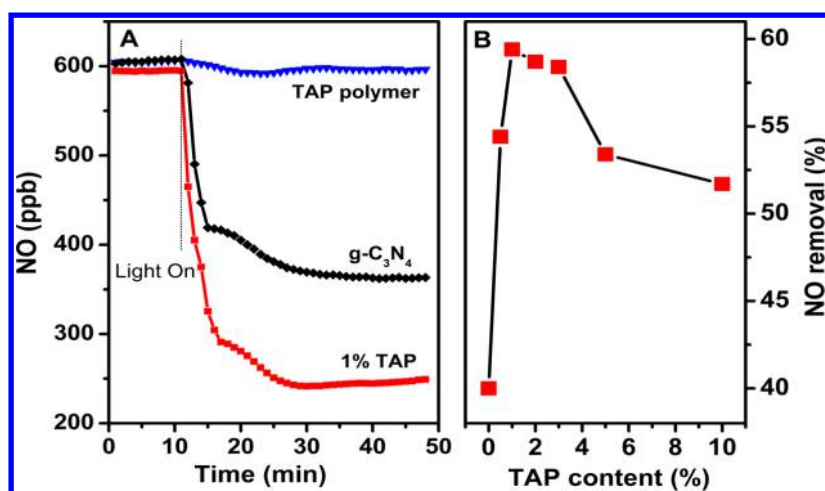


**Figure 7.** (A) Time-online data of NO removal over the pristine and TAP modified  $g\text{-C}_3\text{N}_4$  samples; (B) dependence of TAP content on the photocatalytic activity for NO removal.

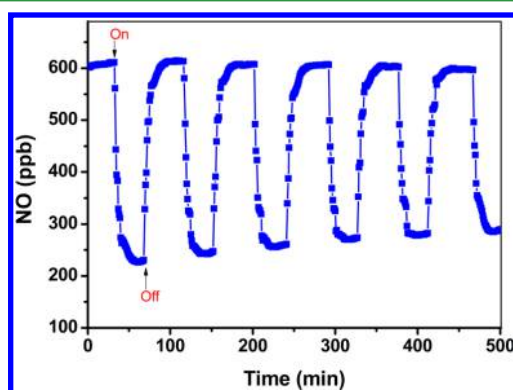


**Figure 8.** Stability of 1% TAP-CN catalysts for NO removal.

photogenerated charge-carriers. The PL spectra of the samples are shown in Figure 9. The pristine  $g\text{-C}_3\text{N}_4$  sample exhibited a

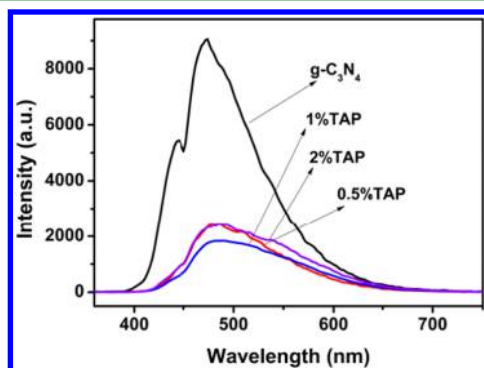


**Figure 9.** PL spectra of the pristine and modified  $g\text{-C}_3\text{N}_4$  samples.

strong and wide luminescence peak centered at about 475 nm, which can be attributed to the band–band PL phenomenon with the energy of light that was approximately equal to the band gap energy of carbon nitride,<sup>30</sup> besides a shoulder peak at shorter wavelength due to some amorphous and low degree of thermal condensation of  $g\text{-C}_3\text{N}_4$ .<sup>31</sup> Obviously, the PL intensity tremendously decreased upon TAP incorporation. PL quenching indicated low recombination rate of the photoinduced charge carriers, which mainly benefited from the decrease of the  $\pi$ -deficiency in the conjugated system by TAP incorporation

and the improved mobility of the free-charge carriers. The low recombination rate of charge carriers has been proposed to facilitate heterogeneous photocatalysis. Moreover, the emission peak in PL for the modified  $g\text{-C}_3\text{N}_4$  samples gradually shifted toward longer wavelength with the continuing increase of TAP content, which is consistent with the narrowing of the band gap energy with TAP incorporation. To confirm the improvement of charge-carrier migration and separation by TAP incorporation, we measured the transient photocurrent of the modified  $g\text{-C}_3\text{N}_4$  (Figure S5 in the Supporting Information). TAP incorporation enhanced the transient photocurrent in comparison with the pristine  $g\text{-C}_3\text{N}_4$ . 1% TAP-CN samples produced the highest photocurrent. The order of the photocurrent of the various TAP incorporation samples was quite in parallel with their photocatalytic activity results reported above.

The sensitive EPR technique was used to investigate the trapped electrons in samples with or without visible light illumination to further determine the influence of TAP incorporation on the photogenerated carriers and the intrinsic electronic structure for  $g\text{-C}_3\text{N}_4$ . Figure 10 shows the X-band EPR spectra of the samples. TAP incorporation increased the EPR spectra of  $g\text{-C}_3\text{N}_4$  in the dark. A single-line EPR spectrum near  $g = 2.0031$  was caused by the generated conduction electrons in the localized  $\pi$  states of  $g\text{-C}_3\text{N}_4$ .<sup>32,33</sup> The existence of these conduction electrons is beneficial to the photocatalytic reactions. The EPR intensities were enhanced when  $g\text{-C}_3\text{N}_4$

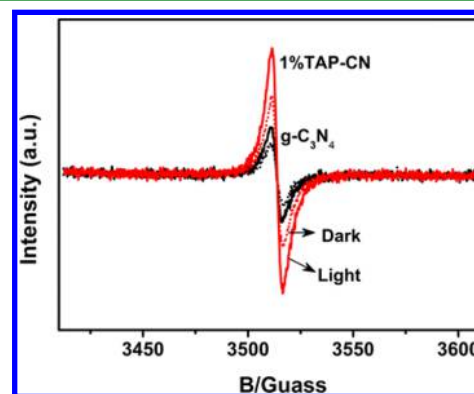


**Figure 10.** EPR spectra of  $g\text{-C}_3\text{N}_4$  and 1%TAP-CN samples in the dark or under visible light ( $\lambda \geq 420$  nm).

and 1%TAP-CN samples were irradiated with visible light. However, the enhanced extent of EPR signal for 1%TAP-CN samples was much more prominent than that for the pristine  $g\text{-C}_3\text{N}_4$ . Therefore, TAP incorporation facilitates the production and separation of photogenerated charge carriers in  $g\text{-C}_3\text{N}_4$  with visible light illumination, which may cause higher photocatalytic activity with the incorporation of TAP.

#### 4. CONCLUSIONS

Precise replacement of nitrogen in triazine ring of polymeric  $g\text{-C}_3\text{N}_4$  with carbon atom was successfully achieved through copolymerization with TAP. The  $g\text{-C}_3\text{N}_4$  photocatalyst showed significant enhancement in activity compared with that of the pristine  $g\text{-C}_3\text{N}_4$ . The integration of  $\text{C}_4\text{N}_2$  ring from TAP molecular into the network of  $g\text{-C}_3\text{N}_4$  not only results in the rolling-up of sheet structure to form nanotube configuration, but also effectively tunes its intrinsic electronic properties by narrowing the band gap energy, hence enhancing the charge-carrier migration and separation. In summary, this study developed a valuable technique for controlling heteroatom doping in the specific site of the network of polymeric  $g\text{-C}_3\text{N}_4$  to improve the intrinsic electronic structures and photocatalytic properties.

#### ■ ASSOCIATED CONTENT

##### Supporting Information

TEM images for 3% TAP-CN, 5%TAP-CN, and 10%TAP-CN; SEM images of the pristine  $g\text{-C}_3\text{N}_4$  and 1% TAP-CN samples; N 1s XPS spectra of 1%TAP-CN samples after NO removal reaction; FT-IR spectra of the 1%TAP-CN samples before and after the prolonged reactions; the periodic on/off photocurrent response of the modified  $g\text{-C}_3\text{N}_4$  samples and computational details. This material is available free of charge via the Internet at <http://pubs.acs.org/>.

#### ■ AUTHOR INFORMATION

##### Corresponding Authors

\*E-mail: keithho@ied.edu.hk.

\*E-mail: z.zhang@fzu.edu.cn.

##### Notes

The authors declare no competing financial interest.

#### ■ ACKNOWLEDGMENTS

This research was financially supported by the research grant of Early Career Scheme (ECS 809813) from the Research Grant Council, Hong Kong SAR Government, Dean's Research Fund-Early Career Researchers (04022), Research Equipment Grant (REG-2), and Internal Research Grant (R3429) from The Hong Kong Institute of Education. This work was also financially supported by the NSFC (Grants 21203029 and U1305242), and the Natural Science Foundation of Fujian Province of PR China (2013J05024), Technology Project of Education Office of Fujian Province of PR China (JA12036 and JA14030) and the CAS Innovation Program of China (Y454031490).

#### ■ REFERENCES

- (1) Wang, X.; Maeda, K.; Thomas, A.; Takanebe, K.; Xin, G.; Carlsson, J. M.; Domen, K.; Antonietti, M. A Metal-free Polymeric Photocatalyst for Hydrogen Production from Water under Visible Light. *Nat. Mater.* **2009**, *8*, 76–80.
- (2) Schwinghammer, K.; Mesch, M. B.; Duppel, V.; Ziegler, C.; Senker, J.; Lotsch, B. V. Crystalline Carbon Nitride Nanosheets for

Improved Visible-Light Hydrogen Evolution. *J. Am. Chem. Soc.* **2014**, *136*, 1730–1733.

- (3) Zhang, J.; Zhang, M.; Yang, C.; Wang, X. Nanospherical Carbon Nitride Frameworks with Sharp Edges Accelerating Charge Collection and Separation at a Soft Photocatalytic Interface. *Adv. Mater.* **2014**, *26*, 4121–4126.

- (4) Jun, Y. S.; Lee, E. Z.; Wang, X.; Hong, W. H.; Stucky, G. D.; Thomas, A. From Melamine-Cyanuric Acid Supramolecular Aggregates to Carbon Nitride Hollow Spheres. *Adv. Funct. Mater.* **2013**, *23*, 3661–3667.

- (5) Zhao, Z.; Dai, Y.; Lin, J.; Wang, G. Highly-Ordered Mesoporous Carbon Nitride with Ultrahigh Surface Area and Pore Volume as a Superior Dehydrogenation Catalyst. *Chem. Mater.* **2014**, *26*, 3151–3161.

- (6) Cao, S.; Yu, J.  $g\text{-C}_3\text{N}_4$ -Based Photocatalysts for Hydrogen Generation. *J. Phys. Chem. Lett.* **2014**, *5*, 2101–2107.

- (7) Wang, X.; Blechert, S.; Antonietti, M. Polymeric Graphitic Carbon Nitride for Heterogeneous Photocatalysis. *ACS Catal.* **2012**, *2*, 1596–1606.

- (8) Cao, Y.; Zhang, Z.; Long, J.; Liang, J.; Lin, H.; Lin, H.; Wang, X. Vacuum Heat-Treatment of Carbon Nitride for Enhancing Photocatalytic Hydrogen Evolution. *J. Mater. Chem. A* **2014**, *2*, 17797–17807.

- (9) Chen, X.; Zhang, J.; Fu, X.; Antonietti, M.; Wang, X. Fe- $g\text{-C}_3\text{N}_4$ -Catalyzed Oxidation of Benzene to Phenol Using Hydrogen Peroxide and Visible Light. *J. Am. Chem. Soc.* **2009**, *131*, 11658–11659.

- (10) Shalom, M.; Inal, S.; Fettkenhauer, C.; Neher, D.; Antonietti, M. Improving Carbon Nitride Photocatalysis by Supramolecular Preorganization of Monomers. *J. Am. Chem. Soc.* **2013**, *135*, 7118–7121.

- (11) Zhao, Z.; Sun, Y.; Dong, F. Graphitic Carbon Nitride Based Nanocomposites: A Review. *Nanoscale* **2014**, *7*, 15–37.

- (12) He, F.; Chen, G.; Yu, Y.; Zhou, Y.; Zheng, Y.; Hao, S. The Sulfur-Bubble Template-Mediated Synthesis of Uniform Porous  $g\text{-C}_3\text{N}_4$  with Superior Photocatalytic Performance. *Chem. Commun.* **2015**, *51*, 425–427.

- (13) Wang, Y.; Bai, X.; Pan, C.; He, J.; Zhu, Y. Enhancement of Photocatalytic Activity of  $\text{Bi}_2\text{WO}_6$  Hybridized with Graphite-Like  $\text{C}_3\text{N}_4$ . *J. Mater. Chem.* **2012**, *22*, 11568–11573.

- (14) Zhao, P.; Wang, B.; Chen, X.; Qian, Y. Carbon Nitride Nanowire Bundle and Tubes: Solid-State Synthesis, Characterization and Photoluminescent Properties. *Chem. Res. Chin. Univ.* **2009**, *25*, 412–416.

- (15) Liu, G.; Niu, P.; Sun, C. H.; Smith, S. C.; Chen, Z. G.; Lu, G. Q.; Cheng, H. M. Unique Electronic Structure Induced High Photo-reactivity of Sulfur-Doped Graphitic  $\text{C}_3\text{N}_4$ . *J. Am. Chem. Soc.* **2010**, *132*, 11642–11648.

- (16) Dong, G.; Zhao, K.; Zhang, L. Carbon Self-Doping Induced High Electronic Conductivity and Photoreactivity of  $g\text{-C}_3\text{N}_4$ . *Chem. Commun.* **2012**, *48*, 6178–6180.

- (17) Zhang, Y.; Mori, T.; Ye, J.; Antonietti, M. Phosphorus-Doped Carbon Nitride Solid: Enhanced Electrical Conductivity and Photocurrent Generation. *J. Am. Chem. Soc.* **2010**, *132*, 6294–6295.

- (18) Yan, S. C.; Li, Z. S.; Zou, Z. G. Photodegradation of Rhodamine B and Methyl Orange over Boron-Doped  $g\text{-C}_3\text{N}_4$  under Visible Light Irradiation. *Langmuir* **2010**, *26*, 3894–3901.

- (19) Wang, Y.; Di, Y.; Antonietti, M.; Li, H.; Chen, X.; Wang, X. Excellent Visible-Light Photocatalysis of Fluorinated Polymeric Carbon Nitride Solids. *Chem. Mater.* **2010**, *22*, 5119–5121.

- (20) Zhang, G.; Zhang, M.; Ye, X.; Qiu, X.; Lin, S.; Wang, X. Iodine Modified Carbon Nitride Semiconductors as Visible Light Photocatalysts for Hydrogen Evolution. *Adv. Mater.* **2013**, *26*, 805–809.

- (21) Wang, Y.; Zhang, J.; Wang, X.; Antonietti, M.; Li, H. Boron- and Fluorine-Containing Mesoporous Carbon Nitride Polymers: Metal-Free Catalysts for Cyclohexane Oxidation. *Angew. Chem., Int. Ed.* **2010**, *49*, 3356–3359.

- (22) Lin, Z.; Wang, X. Nanostructure Engineering and Doping of Conjugated Carbon Nitride Semiconductors for Hydrogen Photosynthesis. *Angew. Chem., Int. Ed.* **2013**, *52*, 1735–1738.

- (23) Zheng, Y.; Liu, J.; Liang, J.; Jaroniec, M.; Qiao, S. Z. Graphitic Carbon Nitride Materials: Controllable Synthesis and Applications in Fuel Cells and Photocatalysis. *Energy Environ. Sci.* **2012**, *5*, 6717–6731.
- (24) Barman, S.; Sadhukhan, M. Facile Bulk Production of Highly Blue Fluorescent Graphitic Carbon Nitride Quantum Dots and Their Application as Highly Selective and Sensitive Sensors for the Detection of Mercuric and Iodide Ions in Aqueous Media. *J. Mater. Chem.* **2012**, *22*, 21832–21837.
- (25) Li, J.; Shen, B.; Hong, Z.; Lin, B.; Gao, B.; Chen, Y. A Facile Approach to Synthesize Novel Oxygen-Doped g-C<sub>3</sub>N<sub>4</sub> with Superior Visible-Light Photoreactivity. *Chem. Commun.* **2012**, *48*, 12017–12019.
- (26) Thomas, A.; Fischer, A.; Goettmann, F.; Antonietti, M.; Müller, J.-O.; Schlögl, R.; Carlsson, J. M. Graphitic Carbon Nitride Materials: Variation of Structure and Morphology and Their Use as Metal-Free Catalysts. *J. Mater. Chem.* **2008**, *18*, 4893–4908.
- (27) Shiraishi, Y.; Kanazawa, S.; Kofuji, Y.; Sakamoto, H.; Ichikawa, S.; Tanaka, S.; Hirai, T. Sunlight-Driven Hydrogen Peroxide Production from Water and Molecular Oxygen by Metal-Free Photocatalysts. *Angew. Chem., Int. Ed.* **2014**, *53*, 13454–13459.
- (28) Zhang, H.; Yu, A. Photophysics and Photocatalysis of Carbon Nitride Synthesized at Different Temperatures. *J. Phys. Chem. C* **2014**, *118*, 11628–11635.
- (29) Heyd, J.; Scuseria, G. E.; Ernzerhof, M. Hybrid Functionals Based on a Screened Coulomb Potential. *J. Chem. Phys.* **2003**, *118*, 8207–8215.
- (30) Li, Y.; Zhang, H.; Liu, P.; Wang, D.; Li, Y.; Zhao, H. Cross-Linked g-C<sub>3</sub>N<sub>4</sub>/rGO Nanocomposites with Tunable Band Structure and Enhanced Visible Light Photocatalytic Activity. *Small* **2013**, *9*, 3336–3344.
- (31) Zhang, Y.; Pan, Q.; Chai, G.; Liang, M.; Dong, G.; Zhang, Q.; Qiu, J. Synthesis and Luminescence Mechanism of Multicolor-Emitting g-C<sub>3</sub>N<sub>4</sub> Nanopowders by Low Temperature Thermal Condensation of Melamine. *Sci. Rep.* **2013**, *3*, 1943/1–7.
- (32) Zhang, J.; Zhang, G.; Chen, X.; Lin, S.; Mchlmann, L.; Dołęga, G.; Lipner, G.; Antonietti, M.; Blechert, S.; Wang, X. Co-Monomer Control of Carbon Nitride Semiconductors to Optimize Hydrogen Evolution with Visible Light. *Angew. Chem., Int. Ed.* **2012**, *51*, 3183–3187.
- (33) Sano, T.; Tsutsui, S.; Koike, K.; Hirakawa, T.; Teramoto, Y.; Negishi, N.; Takeuchi, K. Activation of Graphitic Carbon Nitride (g-C<sub>3</sub>N<sub>4</sub>) by Alkaline Hydrothermal Treatment for Photocatalytic NO Oxidation in Gas Phase. *J. Mater. Chem. A* **2013**, *1*, 6489–6496.